

ATLAS sensitivity to Wtb anomalous couplings in top quark decays

J. A. Aguilar-Saavedra^a, J. Carvalho^b, N. Castro^b, A. Onofre^{b,c}, F. Veloso^b

^a *Departamento de Física Teórica y del Cosmos and CAFPE,
Universidad de Granada, E-18071 Granada, Spain*

^b *LIP - Departamento de Física,
Universidade de Coimbra, 3004-516 Coimbra, Portugal*

^c *UCP, Rua Dr. Mendes Pinheiro 24, 3080 Figueira da Foz, Portugal*

Abstract

We study the sensitivity of the ATLAS experiment to Wtb anomalous couplings in top pair production with semileptonic decay, $t \rightarrow W^+b$, $\bar{t} \rightarrow W^-\bar{b}$ with one of the W bosons decaying leptonically and the other hadronically. Several observables are examined, finding that a convenient choice can significantly reduce systematic uncertainties and improve limits on anomalous couplings by a factor of 1.3–1.7. Combining the most sensitive observables, the precision achieved in the determination of Wtb anomalous couplings is of a few percent in the semileptonic channel alone.

1 Introduction

The three generation structure of the standard model (SM) was completed with the discovery of the top quark at Tevatron [1]. With a mass around 175 GeV, the top is the heaviest and least studied quark. Although its properties have already been directly investigated at colliders [2–5], the available centre of mass (CM) energy and the collected luminosity have not allowed for precise measurements except of its mass [6]. The determination of other fundamental properties, like spin and couplings, requires larger top samples, which will be available at Tevatron Run II and LHC. In its first low luminosity phase (10 fb⁻¹/year), LHC will produce several millions of top quarks per year and experiment, mainly in pairs through gluon fusion $gg \rightarrow t\bar{t}$ and quark-antiquark annihilation $q\bar{q} \rightarrow t\bar{t}$, with a total cross section of 833 pb [7]. Single top production [8,9] will also occur, dominated by the process $bq \rightarrow tq'$, with an expected cross section of 306 pb [7]. Both processes will test the SM predictions for the fundamental properties of the top quark, and in particular they will allow us to measure its couplings [8,10–12]. This

fact is specially important since, from a theoretical point of view, sizeable deviations from the SM predictions for top couplings are possible in several SM extensions.

Within the SM, the Wtb coupling is purely left-handed (at the tree level), and its size is given by the Cabibbo-Kobayashi-Maskawa (CKM) matrix element V_{tb} . In SM extensions, departures from the SM expectation $V_{tb} \simeq 0.999$ are possible [13, 14], as well as new radiative contributions to the Wtb vertex [15, 16]. These deviations might be observed in top production and decay processes at LHC. Top pair production takes place through QCD interactions without involving a Wtb coupling. Additionally, it is likely that the top quark almost exclusively decays in the channel $t \rightarrow W^+b$. Therefore, the cross section for $gg, q\bar{q} \rightarrow t\bar{t} \rightarrow W^+bW^-\bar{b}$ is insensitive to the size and structure of the Wtb vertex. However, the angular distributions of top decay products give information about its structure, and can then be used to probe anomalous top couplings. In the rest frame of a decaying top quark, the energies of the W boson and b quark are fixed by the two-body kinematics. Therefore, non-standard Wtb interactions can only influence:

1. The total width $\Gamma(t \rightarrow Wb)$, which is very difficult to measure.
2. The helicity fractions of the W boson, which are reflected in the angular and energy distributions of its decay products.
3. The angular distribution of the W in top rest frame, with respect to the top spin direction.

The second class of observables, those related to W helicity fractions, may be defined for the decay of a top quark independently of other particles produced, and can be measured in single top as well as in top pair production. In this paper we concentrate on these observables, studying the sensitivity of the ATLAS experiment [17] for their measurement in top pair production and subsequent semileptonic decay. Previous work by the ATLAS collaboration [18] has also addressed these issues. Here we extend this analysis by including new observables [19] for which systematic uncertainties are smaller. (For the observables considered in Ref. [18] similar results are found.) We restrict ourselves to quantities related to the W helicity fractions, and do not study those involving both top and antitop decay products. These are generically less sensitive to anomalous couplings and their study is best suited to explore new physics in the production through the measurement of spin correlations between the top quark pair [20–22].

This paper is organised as follows. In section 2 we briefly discuss the structure of the Wtb vertex and define the observables studied. A more extensive analysis, including

analytical expressions and a comparison with spin-dependent observables, can be found in Ref. [19]. In section 3 the generation of the $t\bar{t}$ signal and backgrounds is outlined, together with the selection criteria used to analyse them. In section 4 we present our results for the experimental measurement of the observables considered, and in section 5 we discuss their implications for the experimental determination of Wtb anomalous couplings. Section 6 is devoted to our conclusions.

2 The effective Wtb vertex and angular distributions in W rest frame

The most general Wtb vertex containing terms up to dimension five can be written as

$$\begin{aligned} \mathcal{L} = & -\frac{g}{\sqrt{2}}\bar{b}\gamma^\mu(V_L P_L + V_R P_R)t W_\mu^- \\ & -\frac{g}{\sqrt{2}}\bar{b}\frac{i\sigma^{\mu\nu}q_\nu}{M_W}(g_L P_L + g_R P_R)t W_\mu^- + \text{h.c.}, \end{aligned} \quad (1)$$

with $q = p_t - p_b$ the W boson momentum. The new anomalous couplings V_R , g_L and g_R [10, 19] can be related to f_1^R , f_2^L and f_2^R in Ref. [18] (and references therein) as $f_1^R = V_R$, $f_2^L = -g_L$ and $f_2^R = -g_R$. If we assume CP is conserved, these couplings can be taken to be real. Within the SM, $V_L \equiv V_{tb} \simeq 0.999$ and the other couplings vanish at the tree level, while nonzero values are generated at one loop level [23]. In models with new physics beyond the SM, departures from these predictions are expected. A moderate deviation from $V_L \simeq 1$ is not visible in top pair production and decay, as long as the top quark mainly decays to W^+b and all other channels are rare. (Single top production at LHC [8, 9], as well as at an international e^+e^- linear collider (ILC) [24, 25], involves a Wtb vertex in the production, and thus can measure V_L .) Its value, which we normalise to unity, sets the global scale for the measurement of V_R , g_L and g_R in top decays. These non-standard couplings can receive radiative contributions from new physics. The size of a V_R term is constrained by the measured rate of $\text{Br}(b \rightarrow s\gamma) = (3.3 \pm 0.4) \times 10^{-4}$ [26]. A right-handed coupling $|V_R| \gtrsim 0.04$ would in principle give a too large contribution to this decay [27] which, however, might be (partially) cancelled with other new physics contributions. Hence, the bound $|V_R| \leq 0.04$ is model dependent and does not substitute a direct measurement of this coupling. For g_L the limits from $b \rightarrow s\gamma$ are of the same order, while for g_R they are much looser [28].

The polarisation of the W bosons produced in the top decay is sensitive to non-standard couplings [29]. W bosons can be produced with positive, negative or zero

helicity, with corresponding partial widths $\Gamma_R, \Gamma_L, \Gamma_0$ which depend on V_L, V_R, g_L and g_R . (General expressions for $\Gamma_R, \Gamma_L, \Gamma_0$ in terms of these couplings can be found in Ref. [19].) Their absolute measurement is rather difficult, so it is convenient to consider instead the helicity fractions $F_i \equiv \Gamma_i/\Gamma$, with $\Gamma = \Gamma_R + \Gamma_L + \Gamma_0$ the total width for $t \rightarrow Wb$. Within the SM, $F_0 = 0.703$, $F_L = 0.297$, $F_R = 3.6 \times 10^{-4}$ at the tree level, for $m_t = 175$ GeV, $M_W = 80.39$ GeV, $m_b = 4.8$ GeV. We note that F_R vanishes in the $m_b = 0$ limit because the b quarks produced in top decays have left-handed chirality, and for vanishing m_b the helicity and the chirality states coincide. These helicity fractions can be measured in leptonic decays $W \rightarrow \ell\nu$. Let us denote by θ_ℓ^* the angle between the charged lepton three-momentum in the W rest frame and the W momentum in the t rest frame. The normalised angular distribution of the charged lepton can be written as

$$\frac{1}{\Gamma} \frac{d\Gamma}{d\cos\theta_\ell^*} = \frac{3}{8}(1 + \cos\theta_\ell^*)^2 F_R + \frac{3}{8}(1 - \cos\theta_\ell^*)^2 F_L + \frac{3}{4}\sin^2\theta_\ell^* F_0, \quad (2)$$

with the three terms corresponding to the three helicity states and vanishing interference [30]. A fit to the $\cos\theta_\ell^*$ distribution allows to extract from experiment the values of F_i , which are not independent but satisfy $F_R + F_L + F_0 = 1$. From these measurements one can constrain the anomalous couplings in Eq. (1). Alternatively, from this distribution one can measure the helicity ratios [19]

$$\rho_{R,L} \equiv \frac{\Gamma_{R,L}}{\Gamma_0} = \frac{F_{R,L}}{F_0}, \quad (3)$$

which are independent quantities and take the tree-level values $\rho_R = 5.1 \times 10^{-4}$, $\rho_L = 0.423$ in the SM. As for the helicity fractions, the measurement of helicity ratios sets bounds on V_R, g_L and g_R .

A third and simpler method to extract information about the Wtb vertex is through angular asymmetries involving the angle θ_ℓ^* . For any fixed t in the interval $[-1, 1]$, one can define an asymmetry

$$A_t = \frac{N(\cos\theta_\ell^* > t) - N(\cos\theta_\ell^* < t)}{N(\cos\theta_\ell^* > t) + N(\cos\theta_\ell^* < t)}. \quad (4)$$

The most obvious choice is $t = 0$, giving the forward-backward (FB) asymmetry A_{FB} [10, 31].¹ The FB asymmetry is related to the W helicity fractions by

$$A_{\text{FB}} = \frac{3}{4}[F_R - F_L]. \quad (5)$$

¹Notice the difference in sign with respect to the definitions in Refs. [10, 31], where the angle $\theta_{\ell b} = \pi - \theta_\ell^*$ between the charged lepton and b quark is used.

Other convenient choices are $t = \mp(2^{2/3} - 1)$. Defining $\beta = 2^{1/3} - 1$, we have

$$\begin{aligned} t = -(2^{2/3} - 1) &\rightarrow A_t = A_+ = 3\beta[F_0 + (1 + \beta)F_R], \\ t = (2^{2/3} - 1) &\rightarrow A_t = A_- = -3\beta[F_0 + (1 + \beta)F_L]. \end{aligned} \quad (6)$$

Thus, A_+ (A_-) only depend on F_0 and F_R (F_L). The SM values of these asymmetries are $A_{\text{FB}} = -0.2225$, $A_+ = 0.5482$, $A_- = -0.8397$. They are very sensitive to anomalous Wtb interactions, and their measurement allows us to probe this vertex without the need of a fit to the $\cos\theta_\ell^*$ distribution. We also point out that with a measurement of two of these asymmetries the helicity fractions and ratios can be reconstructed. For instance, using Eqs. (6) and requiring $F_R + F_L + F_0 = 1$, it is found that

$$\begin{aligned} F_R &= \frac{1}{1 - \beta} + \frac{A_- - \beta A_+}{3\beta(1 - \beta^2)}, \\ F_L &= \frac{1}{1 - \beta} - \frac{A_+ - \beta A_-}{3\beta(1 - \beta^2)}, \\ F_0 &= -\frac{1 + \beta}{1 - \beta} + \frac{A_+ - A_-}{3\beta(1 - \beta)}. \end{aligned} \quad (7)$$

3 Simulation of signals and backgrounds and event selection

The signal and various SM backgrounds are generated using several Monte Carlo programs. The $t\bar{t} \rightarrow W^+bW^-\bar{b}$ events in which one of the W bosons decays hadronically and the other one in the leptonic channel $W \rightarrow \ell\nu_\ell$ (with $\ell = e^\pm, \mu^\pm$), are considered as signal events. (From now on, the W boson decaying hadronically and its parent top quark will be named as “hadronic”, and the W decaying leptonically and its parent top quark will be called “leptonic”.) Any other decay channel of the $t\bar{t}$ pair constitutes a background to this signal. Top pair production, as well as the background from single top production, is generated with TopReX 4.10 [32]. Further backgrounds without top quarks in the final state, i.e. $b\bar{b}$, W +jets, Z/γ^* +jets, WW , ZZ and ZW production processes, are generated using PYTHIA 6.206 [33]. In all cases we use CTEQ5L parton distribution functions (PDFs) [34]. Events are hadronised using PYTHIA, taking also into account both initial state radiation (ISR) and final state radiation (FSR).

Signal and background events are passed through the ATLAS fast simulation program ATLFAST 2.53 [35] for particle reconstruction and momentum smearing. A cone algorithm is used to associate clusters of energy deposits in the calorimeters into jets if their angular difference in the $\eta - \phi$ plane, $\Delta R = \sqrt{(\Delta\phi)^2 + (\Delta\eta)^2}$, is smaller than

0.4. The events are then passed through the ATLFASBTB package to identify the jets which originate in b quarks. The b jet tagging efficiency is set to 60%, that corresponds to a rejection factor of 10 (100) for c jets (light quark and gluon jets).

Signal events have a final state topology characterised by one energetic lepton², at least four jets (including two b jets) and large transverse missing energy from the undetected neutrino. We apply a two-level probabilistic analysis, based on the construction of a discriminant variable which uses the full information of some kinematical properties of the event. In the first level (called the pre-selection), a cleaner sample is obtained accepting events with: (i) exactly one charged lepton with $p_T > 25$ GeV, $|\eta| < 2.5$; (ii) at least 4 jets with $p_T > 20$ GeV, $|\eta| < 2.5$, two of them tagged as b jets and at least two not b -tagged; (iii) missing transverse momentum above 20 GeV. The number of signal and background events (normalised to $L = 10 \text{ fb}^{-1}$) and the signal efficiency after the pre-selection are shown in the first column of Table 1. Distributions of relevant variables are presented in Fig. 1.

Process	Pre-Selection	Final Selection
$t\bar{t} \rightarrow \ell\nu b\bar{b}q\bar{q}'$	262111 (11%)	220024 (9%)
$t\bar{t}$ (other)	36745	27060
Single t	12410	7600
Z +jets	566	253
W +jets	3627	1307
WW, ZZ, ZW	109	51
total SM bkg.	53457	36271

Table 1: Number of signal $t\bar{t} \rightarrow \ell\nu b\bar{b}q\bar{q}'$ and background events, normalised to $L = 10 \text{ fb}^{-1}$, after the pre-selection and final selection.

The hadronic W reconstruction is done from the two non- b jets with highest transverse momentum. The invariant mass of these two jets is represented in Fig. 1 at the pre-selection. The mass of the hadronic top, also shown in Fig. 1, is reconstructed as the invariant mass of the hadronic W and the b jet (among the two with highest p_T) closer to the W . The leptonic W momentum cannot be directly reconstructed due to the presence of an undetected neutrino in the final state. Nevertheless, the neutrino four-momentum can be estimated by assuming the transverse missing energy to be the transverse neutrino momentum. Its longitudinal component can then be determined, with a quadratic ambiguity, by constraining the leptonic W mass (calculated as the

²Only isolated leptons are considered. The isolation criterium requires the absence of additional tracks with $p_T > 10$ GeV inside a cone of $\Delta R = 0.4$ around the lepton direction.

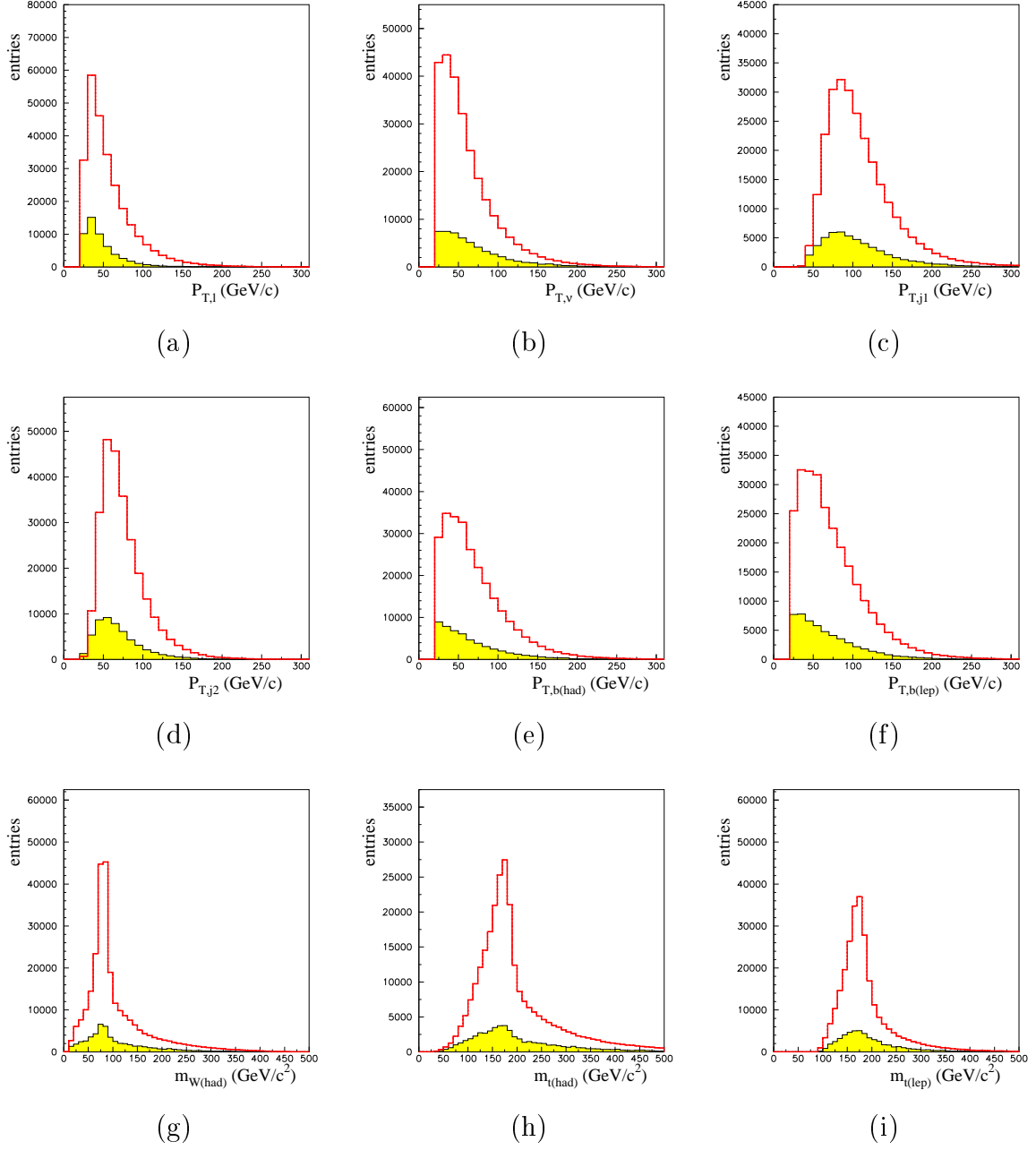


Figure 1: Kinematical distributions at the pre-selection level for the transverse momentum of the charged lepton (a), the neutrino (b), the two highest p_T jets (c),(d), the b jet from the hadronic (e) and leptonic (f) top quarks. Invariant mass distributions of the hadronic W boson (g), the hadronic top (h) and the leptonic top (i). The $t\bar{t}$ signal (full line) and the SM backgrounds (shaded region) are normalised to $L = 10 \text{ fb}^{-1}$.

invariant mass of the neutrino and the charged lepton) to its known on-shell value $M_W \simeq 80.4$ GeV. In order to solve the twofold quadratic ambiguity in the longitudinal component it is required that the hadronic and the leptonic top quarks have the minimum mass difference. The reconstructed mass of the leptonic top is shown in Fig. 1 at the pre-selection.

In the second level (the final selection), for each event we construct signal and background-like probabilities, $\mathcal{P}_i^{\text{signal}}$ and $\mathcal{P}_i^{\text{back.}}$, respectively, using probability density functions (p.d.f.) built from relevant physical variables:

- The hadronic W mass.
- The hadronic and leptonic top masses.
- The transverse momentum of the b -jets associated to the hadronic and the leptonic top quarks.
- The transverse momentum of the jets used in the hadronic W reconstruction.

Signal ($\mathcal{L}_S = \prod_{i=1}^n \mathcal{P}_i^{\text{signal}}$) and background ($\mathcal{L}_B = \prod_{i=1}^n \mathcal{P}_i^{\text{back.}}$) likelihoods (with $n = 7$, the number of p.d.f.) are used to define a discriminant variable $L_R = \log_{10} \mathcal{L}_S / \mathcal{L}_B$. This variable is shown in Fig. 2 for the signal and background. The final event selection is done by applying a cut $L_R > -0.2$ on the discriminant variable, which corresponds to the highest S/\sqrt{B} ratio. The number of background events (normalised to $L = 10$ fb $^{-1}$) and signal efficiency after the final selection are shown in the second column of Table 1.

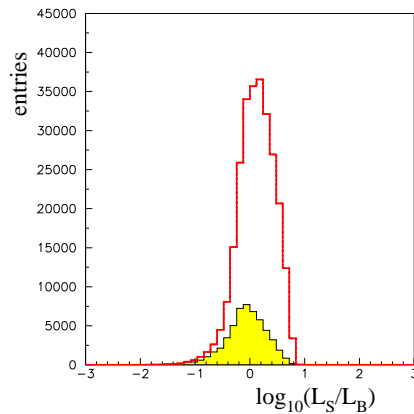


Figure 2: Discriminant variable for the SM background (shaded region) and the $t\bar{t}$ signal (full line), normalised to $L = 10$ fb $^{-1}$.

Two more analyses of sequential type, omitted here for brevity, have also been performed. The results obtained depend more on the top mass reconstruction method than on the type (sequential or probabilistic) of analysis performed. A detailed comparison of the three of them can be found in Ref. [36], where it is shown that the probabilistic analysis presented here gives the best results, with smaller systematic uncertainties.

4 Experimental measurement of angular distributions and asymmetries

The experimentally observed $\cos\theta_\ell^*$ distribution, which includes the $t\bar{t}$ signal as well as the SM backgrounds, is affected by detector resolution, $t\bar{t}$ reconstruction and selection criteria. In order to recover the theoretical distribution, it is necessary to: (i) subtract the background; (ii) correct for the effects of the detector, reconstruction, etc. For this purpose, we use two different sets of signal and background event samples: one “experimental” set, which simulates a possible experimental result, and one “reference” set, which is used to parameterise the effects mentioned and correct the previous sample. The procedure is as follows. After subtracting reference background samples, the “experimental” distribution is multiplied by a correction function f_c in order to recover the theoretical one expected in the SM.³ The correction function is calculated, for each bin of the $\cos\theta_\ell^*$ distribution, dividing the number of events at the generator level by the number of events after the event selection, using the reference sample. The “experimental” $\cos\theta_\ell^*$ distribution obtained after the simulation is shown in Fig. 3, together with the correction function obtained from the reference sample. The asymmetries are measured with a simple counting of the number of events below and above a specific value of $\cos\theta_\ell^*$. The procedure to correct for detector and reconstruction effects is basically the same, but with the $\cos\theta_\ell^*$ distribution divided into two or three bins. This has the advantage that the asymmetry measurements are not biased by the extreme values of the angular distributions, where correction functions largely deviate from unity and special care is required (see Fig. 3). The helicity fractions and ratios obtained from a fit to the corrected distribution, as well as the angular asymmetries A_{FB} , A_\pm , are collected in Table 2, with their statistical uncertainties. For easy comparison, we also include the theoretical values obtained at the generator level.

³Correction functions are determined assuming that the charged lepton distribution corresponds to the SM one. In case that a deviation from SM predictions (corresponding to anomalous couplings) is found, the correction function must be modified accordingly, and the theoretical distribution recalculated in an iterative process. These issues have been analysed in detail in Ref. [18], where it is shown that this process quickly converges.

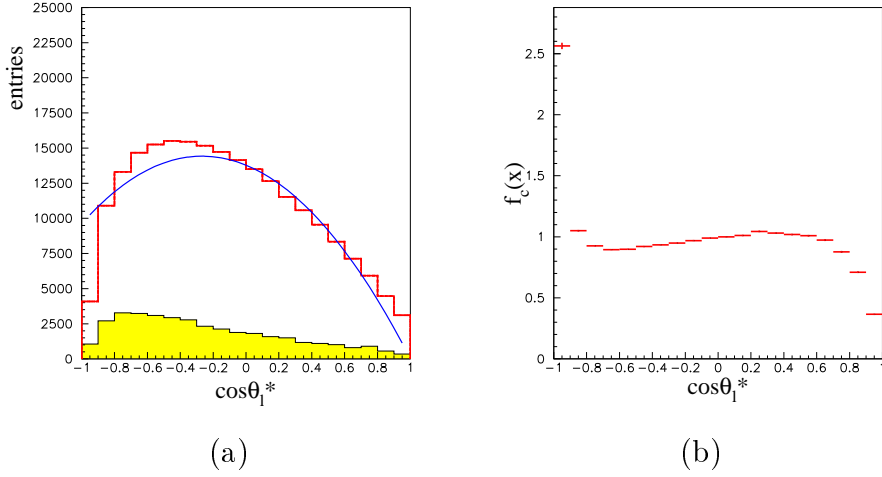


Figure 3: Simulated $\cos\theta_\ell^*$ distribution (a) and its correction function (b). In the first plot the $t\bar{t}$ signal (full line) and the SM backgrounds (shaded region) are normalised to $L = 10 \text{ fb}^{-1}$.

	F_0	F_L	F_R	ρ_L	ρ_R	A_{FB}	A_+	A_-
Th.	0.703	0.297	3.6×10^{-4}	0.423	5.1×10^{-4}	-0.2220	0.5493	-0.8402
Rec.	0.699	0.299	0.0021	0.4274	0.0004	-0.2231	0.5472	-0.8387
$\Delta_{\text{stat.}}$	0.004	0.004	0.0030	0.0080	0.0021	0.0035	0.0032	0.0018

Table 2: Theoretical and reconstructed values of helicity fractions, helicity ratios and angular asymmetries, with their statistical errors for $L = 10 \text{ fb}^{-1}$.

Due to the excellent statistics achievable at LHC, which is apparent in Table 2, systematic errors play a crucial role in the measurement of angular distributions and asymmetries already for a luminosity of 10 fb^{-1} . A thorough discussion of the different systematic uncertainties in the determination of the correction functions is therefore compulsory. We estimate the systematic errors in the observables studied (asymmetries, helicity fractions and ratios) by calculating them with various reference samples and observing the differences obtained. We consider uncertainties originating from:

Monte Carlo generator: The correction functions obtained from a sample generated with TopReX are applied to a sample generated with ALPGEN [37]. The difference between the values obtained at the generator level and after the simulation is considered as systematic uncertainty.

Structure functions: The correction functions obtained from a reference sample generated with CTEQ5L PDFs are applied to samples generated with CTEQ6L and

MRST2001 PDFs in order to estimate the effects on the correction functions, and thus on the observables. The most significant deviations found are considered as the systematic error associated to the structure functions.

Top mass dependence: Samples corresponding to top masses of 170, 175 and 180 GeV are simulated, and the influence of m_t on the values obtained for the corrected observables (using correction functions for $m_t = 175$ GeV) is determined. The systematic error used here is obtained from a linear fit of the values found corresponding to a top mass uncertainty of 2 GeV.

ISR and FSR: Their effect is studied following Ref. [38]. An event sample is created in which ISR and FSR are switched off in the event simulation. We compare the results of the reference sample (with ISR and FSR) with those obtained adding to it a normalised fraction of the sample without ISR nor FSR (from 0% to 25%, in steps of 5%). The values obtained for the observables are fitted with a linear function and the systematic error is considered as the effect of the presence of 20% (a conservative estimate of our level of knowledge of ISR and FSR) of the sample without ISR, FSR.

b jet tag efficiency: The value of the b jet tag efficiency (and the corresponding c jet and light jet rejection factors) is varied from 50 to 70%, in steps of 5%, and the values obtained for the observables are fitted with a linear function. The systematic error is considered as the effect on the observables of a variation of 5% in the b jet tagging efficiency, as compared with the standard value of 60%.

b jet energy scale: The value of the b jet energy scale is changed from -5 to +5%, and the values obtained for the observables are fitted with a linear function. The systematic error is considered as the effect of a variation of 3% in the b jet energy scale.

Light jet energy scale: The value of the energy scale of the light jets is changed from -3 to +3%, and the values obtained for the observables are fitted with a linear function. The systematic error is considered as the effect of a variation of 1% in the energy scale of the light jets.

Background: The background (as obtained from the reference sample) subtracted to the selected sample is varied from -25 to 25%, in steps of 5%, and the values obtained for the observables are fitted with a linear function. The systematic error is considered as the effect of a variation of 10% on the background level (which takes into account the uncertainties in the cross-sections).

Pile-up: The effect of pile-up events (2.3 events in average) is studied by comparing the values of the observables obtained with and without adding pile-up events.

b quark fragmentation: The parameter ϵ_b in the Peterson parameterisation for b

quark fragmentation is changed from -0.006 to -0.0035, and the values obtained for the observables compared. The difference is considered as systematic error [38].

The systematic errors in each observable, resulting from these theoretical and simulation uncertainties, are collected in Table 3. It can be noticed that a convenient choice of observables (ρ_R instead of F_R , A_{\pm} instead of A_{FB}) reduces the total systematic error. The results of our simulation, including statistical and systematic uncertainties, are summarised in Table 4. For F_0 , F_L and F_R they are compatible with those of Ref. [18].

Source	F_0	F_L	F_R	ρ_L	ρ_R	A_{FB}	A_+	A_-
MC generator	0.0018	0.0014	0.0004	0.0006	0.0000	0.0035	0.0015	0.0006
PDFs	0.0045	0.0017	0.0027	0.0046	0.0008	0.0021	0.0005	0.0014
Top mass	0.0065	0.0060	0.0006	0.0124	0.0007	0.0034	0.0039	0.0005
ISR+FSR	0.0142	0.0131	0.0011	0.0218	0.0001	0.0046	0.0049	0.0011
b tag eff.	0.0080	0.0069	0.0011	0.0126	0.0003	0.0039	0.0046	0.0004
E_b scale	0.0019	0.0024	0.0004	0.0061	0.0002	0.0021	0.0017	0.0005
E_j scale	0.0030	0.0038	0.0005	0.0074	0.0002	0.0038	0.0023	0.0014
Back.	0.0002	0.0000	0.0002	0.0001	0.0000	0.0001	0.0000	0.0001
Pile-up	0.0087	0.0084	0.0003	0.0175	0.0002	0.0080	0.0051	0.0006
b frag.	0.0012	0.0015	0.0004	0.0078	0.0011	0.0045	0.0000	0.0012
Total Δ_{sys} .	0.0206	0.0188	0.0033	0.0356	0.0016	0.0130	0.0099	0.0028

Table 3: Sources of systematic errors in the determination of helicity fractions, helicity ratios and angular asymmetries.

Observable	Result		
F_0	0.699	± 0.004 (stat)	± 0.020 (sys)
F_L	0.299	± 0.004 (stat)	± 0.019 (sys)
F_R	0.0021	± 0.0030 (stat)	± 0.0033 (sys)
ρ_L	0.4274	± 0.0080 (stat)	± 0.0356 (sys)
ρ_R	0.0004	± 0.0021 (stat)	± 0.0016 (sys)
A_{FB}	-0.2231	± 0.0035 (stat)	± 0.0130 (sys)
A_+	0.5472	± 0.0032 (stat)	± 0.0099 (sys)
A_-	-0.8387	± 0.0018 (stat)	± 0.0028 (sys)

Table 4: Summary of the results obtained from the simulation for the observables studied, including statistical and systematic uncertainties.

5 Limits on anomalous couplings

With the results obtained in the previous section, summarised in Table 4, and the parametric dependence of the observables on V_R , g_L and g_R implemented in the computer program `TopFit` [19], constraints on the latter can be set. Naively, to obtain the 1σ limit on a coupling $x = V_R, g_L, g_R$ derived from the measurement of some observable O , one would simply find the values of x for which O deviates 1σ from its central value.⁴ Nevertheless, due to the quadratic dependence of the observables on V_R and g_L near the SM point $V_R = g_L = 0$, this procedure leads to overcoverage of the obtained confidence intervals [19], because their p.d.f. is not Gaussian even if the p.d.f. of the observable O is. In order to obtain the limits on an anomalous coupling x , given by the measurement of an observable O , we determine the p.d.f. of x numerically, using the acceptance-rejection method: we iteratively (i) generate a random value (with uniform probability) x_i within a suitable interval; (ii) evaluate the probability of $O(x_i)$, given by the p.d.f. of O ; (iii) generate an independent random number r_i (with uniform probability); and (iv) accept the value x_i if the probability of $O(x_i)$ is larger than r_i . The resulting set of values $\{x_i\}$ is distributed according to the p.d.f. of x given by the measurement of O . The determination of a central interval with a given CL γ is done numerically, requiring: (a) that it contains a fraction γ of the total number of values $\{x_i\}$; (b) that is central, *i.e.* fractions $(1 - \gamma)/2$ of the values generated are on each side of the interval.

For $x = g_R$ this method gives results very similar to the intersection method in Refs. [18,36], whereas for V_R and g_L the confidence intervals found are 20–30% smaller. The 1σ limits derived from the measurement of each observable are collected in Table 5, assuming only one nonzero coupling at a time. We clearly notice the great improvement in sensitivity brought by the new observables $\rho_{R,L}$ and A_{\pm} : the best limits on V_R and g_L are obtained from the measurement of ρ_R , improving the limits from F_R by a factor of 1.7, and the best limits on g_R are provided by A_+ , improving the limits from A_{FB} by a factor of 1.3. This is due to the smaller statistical uncertainties of the new observables and their stronger dependence on anomalous couplings.

These limits can be further improved by combining the measurements of the four observables $\rho_{R,L}$ and A_{\pm} , using their correlation matrix in Table 6 which is obtained from our simulations.⁵ Moreover, the assumption that only one coupling is nonzero

⁴This is the procedure originally followed in our previous work [36], as well as in Ref. [18]: For an observable O and a coupling x , intersecting the plot of $O(x)$ with the two horizontal lines $O = O_{\text{exp}} \pm \Delta O$, which correspond to the 1σ variation of O , gives the pretended 1σ interval on x .

⁵We point out that the correlations among A_{\pm} , $\rho_{R,L}$ do depend (as they must) on the method

	V_R ($g_L = g_R = 0$)	g_L ($V_R = g_R = 0$)	g_R ($V_R = g_L = 0$)
F_0	–	$[-0.141, 0.108]$	$[-0.0367, 0.0228]$
F_L	$[-0.204, 0.191]$	$[-0.175, 0.144]$	$[-0.0309, 0.0231]$
F_R	$[-0.0770, 0.146]$	$[-0.0666, 0.0346]$	–
ρ_L	$[-0.254, 0.206]$	–	$[-0.0275, 0.0227]$
ρ_R	$[-0.0282, 0.0987]$	$[-0.0455, 0.0129]$	–
A_{FB}	$[-0.118, 0.148]$	$[-0.0902, 0.0585]$	$[-0.0268, 0.0227]$
A_+	$[-0.140, 0.146]$	$[-0.112, 0.0819]$	$[-0.0213, 0.0164]$
A_-	$[-0.0664, 0.120]$	$[-0.0620, 0.0299]$	$[-0.0166, 0.0282]$

Table 5: Limits on anomalous couplings obtained by the measurement of the observables in the left column, with the constraint that only one non-standard coupling is allowed to be nonzero at a time. Dashes are shown where there is no significant sensitivity.

can be relaxed. However, if V_R and g_L are simultaneously allowed to be arbitrary, essentially no limits on them can be set, because for fine-tuned values of these couplings their effects on helicity fractions cancel to a large extent. In this way, values $O(1)$ of V_R and g_L are possible yielding minimal deviations on the observables studied. Therefore, in our combined limits, which are presented in Table 7, we require that either V_R or g_L vanishes. In the next section we discuss how one could set limits for both V_R , g_L nonzero.

	A_+	A_-	ρ_L	ρ_R
A_+	1	0.1587	-0.8222	-0.1232
A_-	0.1587	1	-0.08583	0.5688
ρ_L	-0.8222	-0.08583	1	0.3957
ρ_R	-0.1232	0.5688	0.3957	1

Table 6: Correlation matrix for A_{\pm} , $\rho_{R,L}$.

For completeness, and to compare with existing analyses, we also quote the 2σ followed to extract these observables from experiment. In our case, the correlations in Table 6 have been derived with the same procedure used to extract A_{\pm} , $\rho_{R,L}$ from simulated experimental data.

	V_R	g_L	g_R
$A_{\pm}, \rho_{R,L}$	$[-0.0195, 0.0906]$	\times	\times
$A_{\pm}, \rho_{R,L}$	\times	$[-0.0409, 0.00926]$	\times
$A_{\pm}, \rho_{R,L}$	\times	\times	$[-0.0112, 0.0174]$
$A_{\pm}, \rho_{R,L}$	\times	$[-0.0412, 0.00944]$	$[-0.0108, 0.0175]$
$A_{\pm}, \rho_{R,L}$	$[-0.0199, 0.0903]$	\times	$[-0.0126, 0.0164]$

Table 7: Limits on anomalous couplings obtained from the combined measurement of $A_{\pm}, \rho_{R,L}$. In each case, the couplings which are fixed to be zero are denoted by a cross.

limits on non-standard couplings when only one of them is nonzero,

$$\begin{aligned}
V_R (2\sigma) & [-0.0566, 0.128] & (g_L = g_R = 0), \\
g_L (2\sigma) & [-0.0579, 0.0258] & (V_R = g_R = 0), \\
g_R (2\sigma) & [-0.0260, 0.0312] & (V_R = g_L = 0).
\end{aligned} \tag{8}$$

A significant improvement, by factors of 3.25, 3.1 and 1.4, respectively, is obtained with the present analysis with respect to the results presented in Ref [18], which include the dilepton channel as well. This improvement is mainly due to: (i) the better sensitivity of the observables used; (ii) the combination of $\rho_{R,L}$ and A_{\pm} . For V_R and g_L , the Monte Carlo method used to obtain the true 68.3% CL intervals also reduces their size by 20%–30%, as explained above.

Finally, with the same procedure we obtain the 68.3% CL confidence regions on the anomalous couplings, presented in Fig. 4. The boundary of the regions has been chosen as a contour of constant χ^2 . In case that the p.d.f. of V_R and g_L were Gaussian, the boundaries would be ellipses corresponding to $\chi^2 = 2.30$ (see for instance Ref. [39]). In our non-Gaussian case the χ^2 for which the confidence regions have 68.3% probability is determined numerically, and it is approximately 1.83 for the (g_L, g_R) plot and 1.85 for (V_R, g_R) .

6 Conclusions

In this paper we have investigated the ATLAS sensitivity to non-standard Wtb couplings. We have considered several observables: the helicity fractions F_i , helicity ratios $\rho_{R,L}$ and angular asymmetries A_{FB}, A_{\pm} . Although these observables can be defined and measured for any top production process with decay $t \rightarrow Wb \rightarrow \ell\nu b$, we have concentrated on top pair production at LHC with semileptonic decay, with a large cross

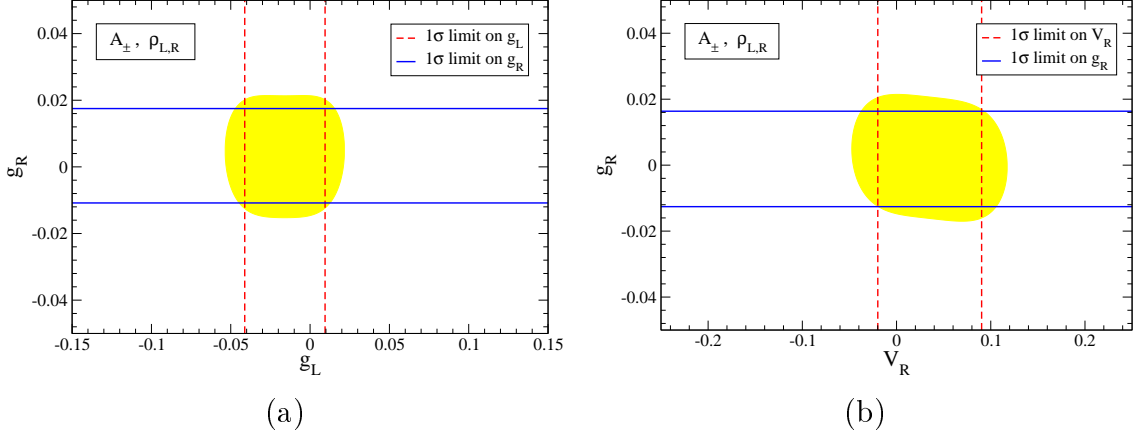


Figure 4: 68.3% CL confidence regions on anomalous couplings: g_L and g_R , for $V_R = 0$ (a); V_R and g_R , for $g_L = 0$ (b). The 1σ combined limits in Table 7 are also displayed.

section and in which the reconstruction of the final state is relatively easy.

Due to the excellent statistics available already with a luminosity of 10 fb^{-1} , the precision reached is determined by systematic uncertainties (theoretical and from the experimental reconstruction). We have performed a very detailed study of systematic uncertainties, finding that, although the observables considered are theoretically equivalent, as noted in section 2, the systematic uncertainties in the measurement of $\rho_{R,L}$ and A_{\pm} are significantly smaller. When these four measurements are combined, the sensitivity to anomalous couplings reaches the 5.5%, 2.5% and 1.4% level for V_R , g_L and g_R in Eq. (1), respectively. This is an important achievement for a hadronic machine. Combining this measurement in $t\bar{t}$ semileptonic decays with the dilepton decay channel $t\bar{t} \rightarrow \ell^+ \nu b \ell'^- \nu \bar{b}$ and single top production will improve (to what extent is yet to be determined) these limits.

Although providing probably the strongest limits, the observables studied in this paper are not sufficient to fully constrain anomalous Wtb couplings in a model-independent way. In the last section we have mentioned that for nonzero V_R and g_L , even of order $O(1)$, there are fine-tuned combinations for which their effects on all these observables almost cancel. The clue to solve this “fine-tuning” problem and set limits simultaneously on the three non-standard couplings can be found in our Introduction. In this paper we have restricted ourselves to observables in the second class only, independent of the top spin. Spin-dependent quantities belonging to the third class (or depending on both the W helicity and angular distribution) can help. Indeed, in the dilepton channel, two spin asymmetries $A_{\ell\ell'}$ and $\tilde{A}_{\ell\ell'}$ [19] involving the two leptons are found to be sensitive to V_R but rather independent of g_L . Ref. [18] has shown that these

asymmetries can be measured with a good precision, 7% and 5%, respectively, and their study seems very promising. Spin asymmetries involving b quarks like $A_{\ell b}$ and $\tilde{A}_{\ell b}$, for which detailed simulations are not still available, exhibit a stronger dependence on anomalous couplings and may be interesting as well.

Acknowledgements

This work has been performed within the ATLAS Collaboration, and we thank collaboration members for helpful discussions. We have made use of the physics analysis framework and tools which are the result of collaboration-wide efforts. The work of J.A.A.-S. has been supported by a MEC Ramon y Cajal contract and project FPA2006-05294, by Junta de Andalucía projects FQM 101 and FQM 437 and by the European Community's Marie-Curie Research Training Network under contract MRTN-CT-2006-035505 "Tools and Precision Calculations for Physics Discoveries at Colliders". The work of J.C., N.C. (grant SFRH/BD/13936/2003), A.O. and F.V. (grant SFRH/BD/18762/2004) has been supported by Fundação para a Ciência e a Tecnologia.

References

- [1] F. Abe *et al.* [CDF Collaboration], Phys. Rev. Lett. **73** (1994) 225 [hep-ex/9405005]; F. Abe *et al.* [CDF Collaboration], Phys. Rev. D **50** (1994) 2966
- [2] V. M. Abazov *et al.* [D0 Collaboration], Phys. Rev. D **72** (2005) 011104 [hep-ex/0505031]; A. Abulencia *et al.* [CDF-Run II Collaboration], Phys. Rev. D **73** (2006) 111103 [hep-ex/0511023]
- [3] F. Abe *et al.* [CDF Collaboration], Phys. Rev. Lett. **80** (1998) 2525
- [4] B. Abbott *et al.* [D0 Collaboration], Phys. Rev. Lett. **85** (2000) 256 [hep-ex/0002058]
- [5] A. Abulencia *et al.* [CDF - Run II Collaboration], hep-ex/0606017; V. M. Abazov *et al.* [D0 Collaboration], Phys. Lett. B **626** (2005) 55 [hep-ex/0505082]
- [6] E. Brubaker *et al.*, [Tevatron Electroweak Working Group], hep-ex/0603039; see also <http://tevewwg.fnal.gov>

- [7] M. Beneke *et al.*, [hep-ph/0003033](#)
- [8] T. Stelzer, Z. Sullivan and S. Willenbrock, Phys. Rev. D **58** (1998) 094021 [[hep-ph/9807340](#)]
- [9] A.S. Belyaev, E. E. Boos and L. V. Dudko, Phys. Rev. D **59** (1999) 075001 [[hep-ph/9806332](#)]; T. Tait and C. P. Yuan, Phys. Rev. D **63** (2001) 014018 [[hep-ph/0007298](#)]
- [10] F. del Aguila and J. A. Aguilar-Saavedra, Phys. Rev. D **67** (2003) 014009 [[hep-ph/0208171](#)]
- [11] D. Espriu and J. Manzano, Phys. Rev. D **66** (2002) 114009 [[hep-ph/0209030](#)]
- [12] C. R. Chen, F. Larios and C. P. Yuan, Phys. Lett. B **631** (2005) 126 [[hep-ph/0503040](#)]
- [13] J. A. Aguilar-Saavedra, Phys. Rev. D **67** (2003) 035003 [[hep-ph/0210112](#)] [Erratum-ibid. D **69** (2004) 099901]
- [14] F. del Aguila and J. Santiago, JHEP **0203** (2002) 010 [[hep-ph/0111047](#)]
- [15] J. j. Cao, R. J. Oakes, F. Wang and J. M. Yang, Phys. Rev. D **68** (2003) 054019 [[hep-ph/0306278](#)]
- [16] X. l. Wang, Q. l. Zhang and Q. p. Qiao, Phys. Rev. D **71** (2005) 014035 [[hep-ph/0501145](#)]
- [17] ATLAS collaboration, *ATLAS detector and physics performance technical design report*, CERN-LHCC-99-15
- [18] F. Hubaut, E. Monnier, P. Pralavorio, K. Smolek and V. Simak, Eur. Phys. J. C **44S2** (2005) 13 [[hep-ex/0508061](#)]
- [19] J. A. Aguilar-Saavedra, J. Carvalho, N. Castro, A. Onofre and F. Veloso, Eur. Phys. J. C **50** (2007) 519 [[hep-ph/0605190](#)]
- [20] T. Stelzer and S. Willenbrock, Phys. Lett. B **374** (1996) 169 [[hep-ph/9512292](#)]
- [21] G. Mahlon and S. J. Parke, Phys. Rev. D **53** (1996) 4886 [[hep-ph/9512264](#)]
- [22] W. Bernreuther, A. Brandenburg, Z. G. Si and P. Uwer, Nucl. Phys. B **690** (2004) 81 [[hep-ph/0403035](#)]

- [23] H. S. Do, S. Groote, J. G. Korner and M. C. Mauser, Phys. Rev. **D 67** (2003) 091501 [[hep-ph/0209185](#)]
- [24] E. Boos, M. Dubinin, A. Pukhov, M. Sachwitz and H.J. Schreiber, Eur. Phys. J. **C 21** (2001) 81 [[hep-ph/0104279](#)]
- [25] P. Batra and T. M. P. Tait, Phys. Rev. D **74** (2006) 054021 [[hep-ph/0606068](#)]
- [26] S. Eidelman *et al.* [Particle Data Group], Phys. Lett. B **592** (2004) 1
- [27] F. Larios, M. A. Perez and C.P. Yuan, Phys. Lett. **B 457** (1999) 334 [[hep-ph/9903394](#)]; G. Burdman, M. C. Gonzalez-Garcia and S. F. Novaes, Phys. Rev. **D 61** (2000) 114016 [[hep-ph/9906329](#)]; K. Whisnant, J. M. Yang, B. L. Young and X. Zhang, Phys. Rev. **D 56** (1997) 467 [[hep-ph/9702305](#)]
- [28] M. Misiak, private communication, to appear in the proceedings of the workshop “Flavour in the era of the LHC”, CERN 2005-2007
- [29] G. L. Kane, G. A. Ladinsky and C. P. Yuan, Phys. Rev. **D 45** (1992) 124
- [30] R. H. Dalitz and G. R. Goldstein, Phys. Rev. **D 45** (1992) 1531
- [31] B. Lampe, Nucl. Phys. **B 454** (1995) 506
- [32] S. R. Slabospitsky and L. Sonnenschein, Comput. Phys. Commun. **148** (2002) 87 [[hep-ph/0201292](#)]
- [33] T. Sjostrand, P. Eden, C. Friberg, L. Lonnblad, G. Miu, S. Mrenna and E. Norrbin, Comput. Phys. Commun. **135** (2001) 238 [[hep-ph/0010017](#)]
- [34] H. L. Lai *et al.* [CTEQ Collaboration], Eur. Phys. J. **C 12** (2000) 375 [[hep-ph/9903282](#)]
- [35] E. Richter-Was, D. Froidevaux and L. Poggioli, ATLAS note ATL-PHYS-98-131
- [36] J. A. Aguilar-Saavedra, J. Carvalho, N. Castro, A. Onofre and F. Veloso, ATLAS note ATL-PHYS-PUB-2006-018
- [37] M. L. Mangano, M. Moretti, F. Piccinini, R. Pittau and A. D. Polosa, JHEP **0307** (2003) 001 [[hep-ph/0206293](#)]; See also <http://mlm.home.cern.ch/m/mlm/www/alpgen/>
- [38] I. Borjanovic *et al.*, Eur. Phys. J. C **39S2** (2005) 63 [[hep-ex/0403021](#)]
- [39] G. Cowan, *Statistical Data Analysis*, Oxford University Press, Clarendon, 1998